Yerbilimleri, 2017, 38 (3), 229-240
Hacettepe Üniversitesi Yerbilimleri Uygulama ve Araştırma Merkezi Bülteni
Bulletin of the Earth Sciences Application and Research Centre of Hacettepe University

Preliminary Investigating results from Azimuthal Seismic Anisotropy beneath Western Anatolia and the Hellenic Subduction Zone

Batı Anadolu'daki Azimutal Sismik Anizotropi ve Helenik Yitim Bölgesinden Ön İnceleme sonuçları

GÜLTEN POLAT[1]*, NURCAN MERAL ÖZEL[1], STUART CRAMPIN[2, 3]

[1]Department of Geophysics, Kandilli Observatory and Earthquake Research Institute
Boğaziçi University, Istanbul – Turkey.

[2]British Geological Survey, The Lyell Centre, Edinburgh EH14 4AP, Scotland UK.

[3]School of Geosciences, University of Edinburgh, Edinburgh EH9 3FW, Scotland UK.

Geliş *(received)* : 22 Ağustos (August) 2016
Kabul *(accepted)* : 19 Kasım (November) 2017

ABSTRACT

To understand the dynamics of a subduction zone, seismic anisotropy is often used, despite the difficulty of constraining anisotropy in the sub-slab region. However, particularly due to constraints imposed by deformation patterns in the mantle surrounding subducting slabs, seismic anisotropy is usually chosen as a better tool. In this study, the dynamics and kinematics of the Hellenic subduction zone and its impact on mantle convection related deformation are investigated by using source-side seismic anisotropy. To this aim, shear wave splitting parameters of local and teleseismic S waves from intermediate and shallow earthquakes are measured. Then, they are combined with splitting parameters obtained from teleseismic SKS and SKKS waves in order to determine variations in seismic anisotropy with depth. Although in the study area strong deep earthquakes are not available, our preliminary splitting results are quite reliable. Also, they are fairly consistent with the presence of azimuthal seismic anisotropy in the asthenosphere below the slab. The averaged fast polarization directions obtained from the analysed teleseismic events show N-S orientations. Additionally, we observed that S-wave fast polarization directions are nearly parallel to the present extension direction of Western Anatolia. It might be suggested that anisotropy may localize within the lower crust, but does not appear to be associated with the present lithospheric extension. Average delay time of teleseismic SKS is greater than 1 s.

Keywords: Source side anisotropy; shear wave splitting; subduction zone; Aegean region.

ÖZ

Yitim zonu dinamiklerini anlamak için yitim alt zonu bölgesindeki anizotropi sınırlandırılmasındaki zorluklara rağmen, sismik anizotropi sıklıkla kullanılmaktadır. Bununla birlikte, özellikle dalan plakayı çevreleyen mantodaki deformasyon modelleri getirdiği kısıtlamalar nedeniyle sismik anizotropi genellikle daha iyi sonuç veren bir araç olarak seçilmiştir. Bu çalışmada, Helenik yitim zonu dinamik ve kinematikleri ile bunların manto konveksiyonu üzerindeki deformasyona bağlı etkileri kaynak - taraflı sismik anizotropi kullanılarak incelenmiştir. Bu amaçla, orta ve sığ depremler yerel ve telesismik S dalgalarının kayma dalgası ayrımlanma parametreleri ölçülmüştür. Daha sonra bunlar, sismik anizotropide derinliğe bağlı değişiklikleri saptamak amacıyla telesismik SKS ve SKKS dalgalarından elde edilen bölme parametreleri ile birleştirilmiştir. Çalışma alanında büyük magnitüdlü derin depremler mevcut olmamasına rağmen, elde ettiğimiz ilk sonuçlar oldukça güvenilirdir. Ayrıca, bu sonuçlar levhanın altında astenosferin içinde azimuthal sismik anizotropi varlığı ile oldukça tutarlıdır. Analiz edilen telesismik olaylardan elde edilen ortalama hızlı polarizasyon yönleri K-G doğrultularını göstermektedir. Ayrıca, S-dalgası hızlı polarizasyon doğrultusunun neredeyse Batı Anadolu'nun bugünkü uzantısı yönüne paralel olduğu görülmüştür. Bu durum, muhtemelen anizotropinin alt kabuk içinde lokalize olabileceği izlenimini vermekle birlikte mevcut litosfer uzantısı ile ilişkili görünmemektedir..

Anahtar Kelimeler: *kaynak-yanı anizotropi, kesme dalgası ayrımlanması, yitim zonu, Ege bölgesi.*

* G. Polat
e-posta: gultenpolat2005@gmail.com

Introduction

Numerous seismological studies (e.g., Lynner and Long, 2014) indicated that the elastic seismic anisotropy is an ubiquitous property of the earth and manifests itself in the seismic wavefield in a variety of ways, including both body waves and surface waves (e.g., Polat et al., 2012). For detecting seismic anisotropy within the earth, shear wave splitting is generally used as a common tool because it is a clear indicator of the anisotropic structure of the earth and is generally unaffected by isotropic wave speed heterogeneity (e.g., Silver, 1996; Savage, 1999; Long and Silver, 2009). Routine shear wave splitting measurements yield high-lateral resolution estimates of polarization of the fast wave (ϕ) and of the delay time ($\delta\tau$) between fast and slow waves (Savage, 1999). The seismic anisotropy of a medium can be characterized by these parameters. The parameter ϕ, or fast axis direction, is the polarization azimuth of the fast shear wave and it corresponds to the alignment of fast axes of anisotropic minerals such as olivine in mantle or fractures. In addition, amount of the parameter $\delta\tau$ is related to the strength and extent of the anisotropy.

Therefore, seismic anisotropy can assist us to learn about mantle flow and deformation because anisotropy is directly related to strain induced LPO (lattice preferred orientation). So far, available anisotropy studies show that anisotropy in seismic velocities can be mainly caused by alignment of elastically anisotropic crystals (rock fabric or LPO) (e.g., Christensen, 1984; Zhang and Karato, 1995), by alignment of fluid-filled pockets (e.g., Zatsepin and Crampin 1997; Crampin, 1978), or by parallel layers of rocks with different physical (isotropic or anisotropic) properties (Backus, 1962; Armstrong et al., 1995). Seismic anisotropy in the upper mantle is nearly always interpreted as being due to the lattice or crystallographic preferred orientation of intrinsically anisotropic minerals such as olivine (e.g., Meissner et al., 2006). LPO will develop when mantle materials are deformed in the dislocation creep regime, which corresponds to a non-Newtonian rheology. Because olivine is the primary constituent of the upper mantle and has a large (~18%) intrinsic shear wave anisotropy, olivine LPO is thought to make the primary contribution to anisotropy observations (e.g., Karato et al., 1995). A number of previous studies (e.g., Hall et al., 2000; Faccenda and Capitanio, 2012, 2013) indicated that strain-induced LPO development can be simulated if the prevalent translation between seismic anisotropy observations and mantle flow direction through mineral physics is available. This approach has been successful used to find out tectonic settings of subduction zones (e.g., Di Leo et al., 2014). Di Leo et al. (2014) constructed an integrated model to simulate history-dependent upper mantle LPO development and resulting shear wave splitting. They concluded that incorporating the entire strain history of the deformed mantle is significant because LPO textures not only change as a function of the magnitude of accumulated finite strain, but also the variation of flow velocity gradients along the path a volume of rock.

In certain regions of the upper mantle, including the mantle wedge of subduction zones, there may be a contribution from other factors such as the shape preferred orientation (SPO) of partial melt (e.g., Ando et al., 1980; Zimmerman et al., 1999; Vauchez et al., 2000). The presence of upper mantle anisotropy in subduction zones has been well documented (e.g., Ando et al., 1983; Long and van der Hilst, 2005), but despite advances in our understanding of the structure of subducting slabs, the character of anisotropy and the pattern of mantle flow in subduction zones remain poorly understood. Previous studies of subduction zone anisotropy have yielded a wide variety of shear wave splitting patterns, including fast directions that are parallel, perpendicular, and (less often) oblique to the trench and a wide range of observed delay times. This is observable because seismic waves are strongly sensitive to the varying elastic properties along their travel paths. A variety of factors from large-scale (e.g. aligned faults, layering) features to small-scale (e.g. aligned cracks and crystals) features may cause seismic anisotropy. As mentioned above, studies have shown that anisotropy in the upper mantle appears to be dominated by LPO of mantle minerals, primarily olivine (e.g., Mainprice, 2007; Karato et al., 2008), which results from deformation. Because of the causative link between dynamic processes in the upper mantle and the resulting anisotropy, the characterization of anisotropy using tools such as shear wave splitting can be used to gain valuable information particularly about the geometry of mantle flow.

Thanks to the increase in the number of deployed seismic stations, detailed studies of the dynamics of the sub-slab mantle have recently been done (e.g., Long and Silver, 2009; Hicks et al., 2012; Eakin et al., 2015; Lynner et al., 2017). Such studies help us to

understand the dynamics of the sub-slab mantle and why trench-parallel anisotropy has been developed beneath subducting slabs (e.g., Russo and Silver, 1994; Lynner and Long, 2014). The observation of Lynner and Long (2014) is striking, as it contravenes the predictions of the simplest two-dimensional models of sub-slab flow and the simplest scenarios for olivine lattice preferred orientation (LPO). They show that the major outstanding question is whether the sub-slab mantle remains strongly coupled to the subducting slab, resulting in an entrained mantle layer, or whether the slab and the surrounding mantle are sufficiently decoupled to allow for escape or 3-D return flow.

In this study, seismic anisotropy beneath Western Anatolia and the Hellenic Subduction Zone is investigated. Similar study was done by Hatzfeld et al. (2001) and Evangelidis et al. (2011). The studies show that this region is an ideal setting for studying subduction dynamics. Although such studies have been done for the subduction zone, the detailed structure of both the slab and the surrounding mantle remain poorly constrained in an intermediate depth range from 30 to ~150 km. Therefore, we used the shear wave splitting method for improving our understanding of the dynamic interaction between subducting lithosphere and the surrounding mantle beneath Western Anatolia and particularly the Hellenic Subduction Zone (Figure 1). In this paper, preliminary results of the study are presented.

Data and Methods

In this study, to measure teleseismic SKS, local and teleseismic S splitting parameters, seismic signals of teleseismic SKS/SKKS, local and teleseismic S phases are picked up from individual seismograms recorded by three component digital broadband stations operated by Boğaziçi University, Kandilli Observatory and Earthquake Research Institute (KOERI) and one permanent station, Isparta (ISP), from the GEOFON network (Figure 2). The stations are equipped with broadband CMG-3TD, CMG-6TD, CMG-3ESPD, CMG-40TD, STS-2 seismometers. SKS and SKKS phases from events at all depths with epicentral distances between 85° and 140° were collected for the stations shown in Figure 2. In addition to this, for local S splitting analysis, local events re-

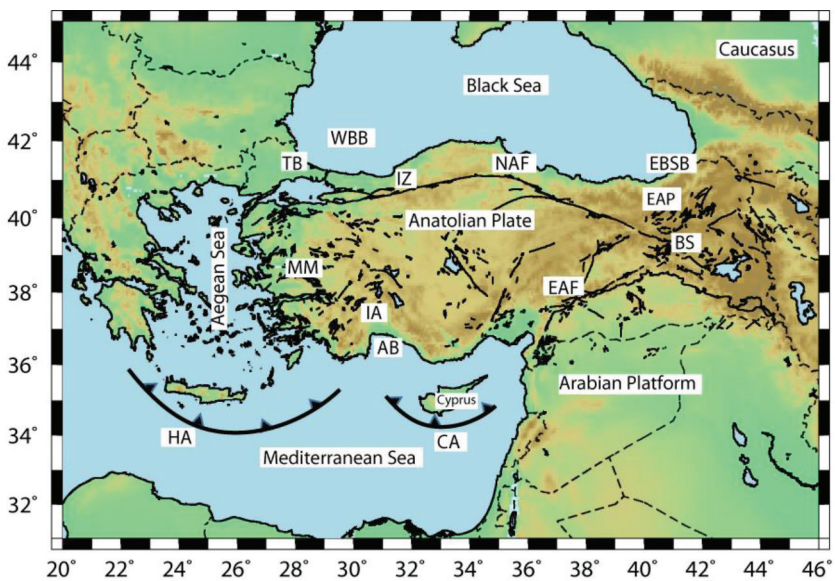

Figure 1. Tectonic map of the study area: AB: Antalya Basin; BS: Bitlis Suture; EAF: East Anatolian Fault; EAP: Eastern Anatolia Plateau; EBSB: Eastern Black Sea Basin; IA: Isparta Angle; HA: Hellenic Arc; CA: Cyprus Arc , IZ: Istanbul Zone; MM: Menderes Massif; NAF: North Anatolian Fault; TB: Thrace Basin and WBB: Western Black Sea Basin.

Şekil 1. Çalışma bölgesinin tektonik haritası. AB: Antalya Havzası; BS: Bitlis Sütürü; DAF: Doğu Anadolu Fayı; DAP: Doğu Anadolu Platosu DKDB: Doğu Karadeniz Havzası; IA) Isparta Büklümü; HA: Helenik Yayı; KA: Kıbrıs Yayı; IZ: Istanbul Zonu; MM: Menderes Masifi; KAF: Kuzey Anadolu Fayı; TB: Trakya Havzası ve BKDB: Batı Karadeniz Havzası.

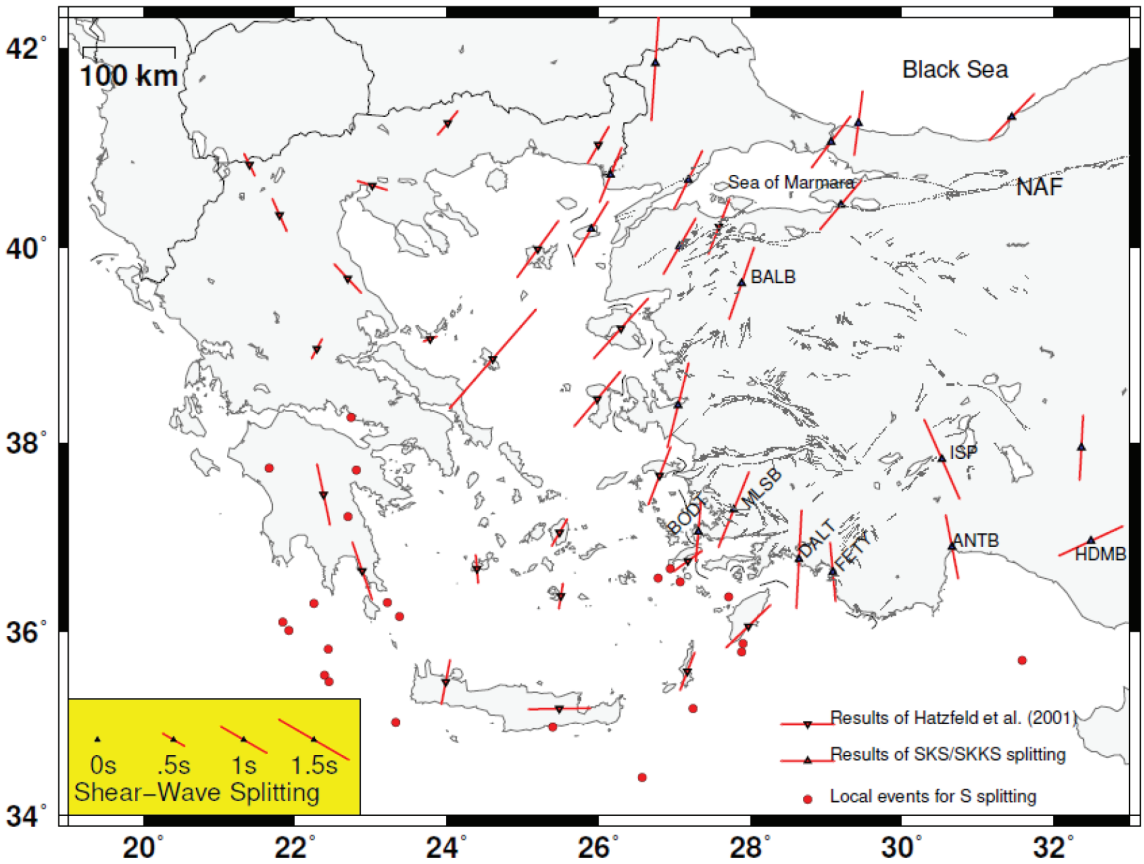

Figure 2. Red circles show the selected local events used in this study. High quality fast directions and time-delays from SKS and SKKS measurements are averaged at each station. The length of bars is proportional to $\delta\tau$. Each red bar represents an average measurement.

Şekil 2. Kırmızı daireler, bu çalışmada kullanılan seçili yerel olayları göstermektedir. SKS ve SKKS ölçümlerinden elde edilen yüksek kaliteli hızlı yönler ve zaman gecikmeleri kullanılarak her bir istasyon için ortalama değerler hesaplanmıştır. Çubukların uzunluğu $\delta\tau$ (zaman gecikme) ile orantılıdır. Her kırmızı ve yeşil çubuk ortalama bir ölçümü temsil eder.

corded by the seismic stations shown in Figure 2 are collected. Distance between the recorder and the source should be smaller than depth of focus of the source. This criterion is strictly considered to identify clearly the impulsive character of the S-wave on the seismogram. The shear-wave splitting analysis is conducted on waveforms generated by earthquakes that are within the shear-wave window. To avoid contamination from S-to-P-phase conversions near the surface, the incident angle of a ray path must be less than the critical angle ic = $\sin^{-1}$(Vs/Vp) with Vp and Vs being the near-surface velocities of P- and S–waves, respectively (Nuttli, 1961; Booth and Crampin, 1985). For a homogeneous half-space with a Poisson's ratio of 0.25, the critical angle is ic ~ 35° (Nuttli, 1961). Because the low-velocity, near-surface layer significantly bends ray paths toward the vertical, a straight straight-line incident angle of 45° is adopted as the critical angle in this study (e.g. Shih and Meyer, 1990; Cochran et al., 2003). The mentioned phases are shown in Figure 3. Magnitudes and depths of local S phases of events are greater than 4.5 and 29.0 km, respectively. In addition to them, distances of the events are less than 10°. To provide better azimuthal coverage for the splitting measurements, same criteria are also applied to select teleseismic S phase waveforms except the distance criterion. The earthquake distances of the teleseismic phases are greater than 10°.

Epicentral distance is also a very significant criterion for teleseismic SKS and SKKS wave splitting analysis. Core phases such as SKS, PKS, and SKKS are

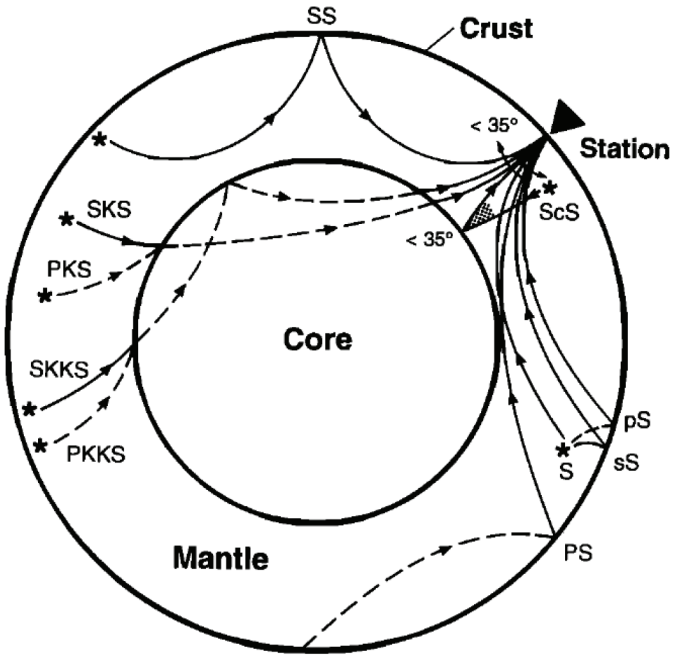

Figure 3. Phases that have been used for shear wave splitting studies. Solid lines are S path segments, dashed lines are P path segments, and stars are earthquake sources. The shear wave window of 35° at the surface and at the core-mantle boundary ensures phases with smaller incidence angles will yield linear S wave particle motion for isotropic propagation (from Savage, 1999).

Şekil 3. Kesme dalgası ayrımlanma çalışmaları için kullanılan aşamalar. S yol parçaları düz çizgilerle, P yol parçaları kesik çizgilerle ve deprem kaynakları yıldızlarla gösterilmiştir. Yüzeyde ve çekirdek-manto sınırındaki 35°' lik pencere ile daha düşük insidans açıları oluşturularak izotropik yayılma için doğrusal S dalga parçacık hareketleri sağlayacaktır.

easily observed beyond 85° as the phases avoid the contamination by other phases, such as S, sS, and ScS (Figure 3). Therefore, data from all the events with the epicentral distance in the range of 85 to 140° are selected. For this, events of magnitude ≥ 5.8 Mw were selected at these epicentral distances. In addition, Hypocentral depth is not an important criterion for teleseismic shear wave splitting.

In this research, the splitting parameters of SKS and SKKS waves are measured by using the transverse component minimization method of Silver and Chan (1991). The method is based upon the principle that a shear wave is linearly polarized in the absence of anisotropy and that passage through an anisotropic medium might result in significant energy on the transverse component and an elliptical particle motion, which is indicative of shear wave splitting. The method performs a grid search over all possible values of ϕ and $\delta\tau$ (up to a reasonable maximum delay time value, usually ~ 4 s), rotates and time-shifts the horizontal components appropriately, and measures the amount of energy on the corrected transverse component, producing a contour plot of transverse component energy for all possible pairs of splitting parameters. The best-fitting parameters correspond to the minimum on this contour plot; formal errors on the measurements are calculated using the inverse F test (Silver and Chan, 1991) and represent the 95% confidence level (and are thus approximately 2 standard deviations). The test is thus performed for each set of possible parameters to determine whether or not the shear wave splitting parameters are within the bounds of the confidence region.

Firstly, shear-wave analysis window is manually selected because visual inspection of individual waveforms is more reliable and preferable than partially or fully automated process (.e.g., Teanby et al., 2004) even though taking spending much more researcher time. For a high quality measurement, energy on both radial and transverse original waveforms should be clearly visible. Before and after splitting corrections, particle motions should be strongly elliptical

and linear, respectively. In addition, contour plots of the transverse component energy should have a small region of minimum energy and 95% confidence level must be small, i.e. ≤ 25 for σσ and 0.2 s for σ. In addition to this, low quality measurements are defined by: 1) signal to noise ratio is lower than 5, but should be more than 2 to see anisotropic energy on raw radial and transverse components, 2) original particle motion is weakly elliptical, 3) the particle motion of the corrected waveforms are only partly linear, 4) formal error in σ is ± 30° and in σt is greater than ±0.2 s. For low quality measurements, visual inspection is given more importance than the formal error. But elliptical particle motion of the original SKS and SKKS phases and linear particle motion of the corrected seismograms are very poor, so it is evaluated as a poor quality measurement. Here the mentioned criteria are strictly considered as evaluating splitting parameters.

In addition to them, to measure the splitting parameters for both local and teleseismic S waves, the smaller of the two eigenvalues in the horizontal covariance matrix (e.g., Silver and Chan, 1991) is minimized. Minimizing the second Eigenvalue of the horizontal covariance matrix provides us to make no a priori assumptions about the initial polarization direction of the shear wave. Hence, by using this method lateral S wave velocity heterogeneity's influence on anisotropy are able to be considered. However, this method is not as well as the minimization of the tangential component.

The horizontal covariance matrix is defined as:

$$C_{ij} = \sum_{k=1}^{N} \left(u_i(k - n \pm \delta t) * u_j(k)\right) \qquad \text{eq.1}$$

In eq.1, n is the sampling rate, N is the total number of data points for the given time series and k is the digital time index. The is the delay time and u is a split shear wave (see Silver and Chan, 1991 for detail information about the equation).

It is well known that shear wave splitting is a measure of the integrated effects of all anisotropic media along the entire ray path. Therefore, it is not easy to confine the depth of seismic anisotropy. However, in this

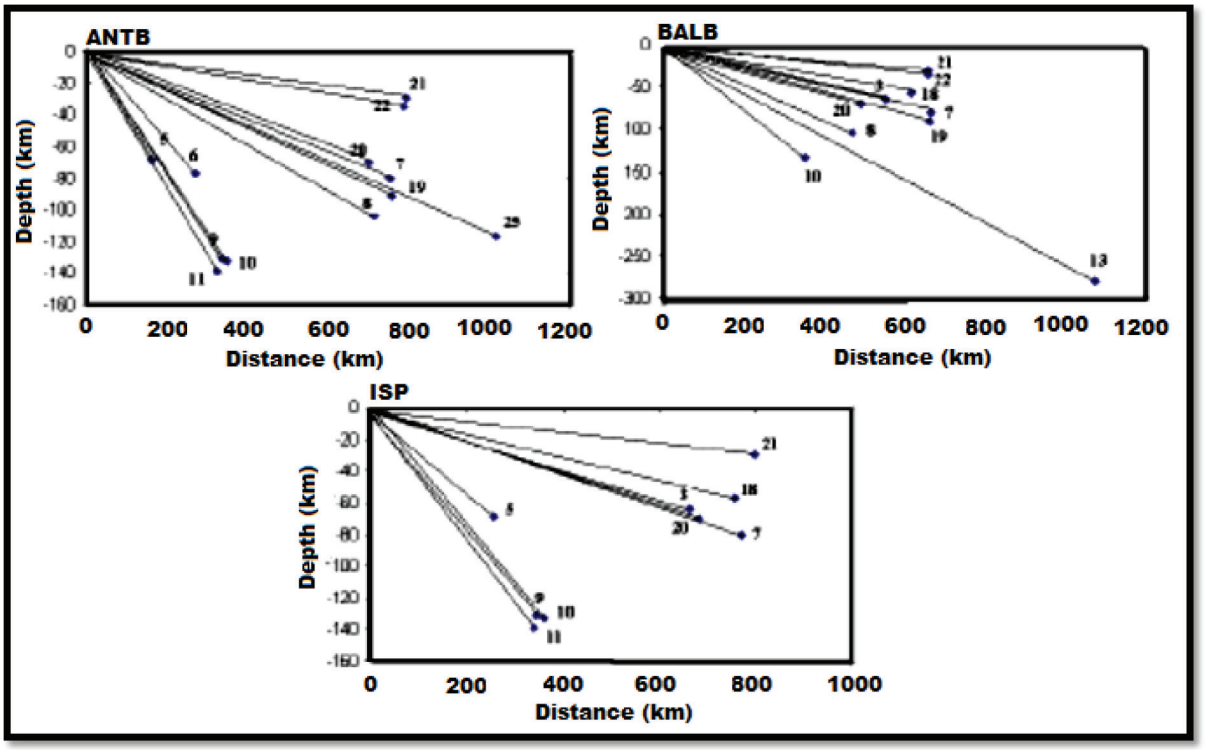

Figure 4. Events used in this study are displayed as a function of depth and distance for each station. The used earthquakes are not illustrated with true sections. The numbers correspond with those in Table 1.

Şekil 4. Bu çalışmadaki olaylar, her bir istasyon için derinlik – mesafe fonksiyonu olarak gösterilmiştir. Kullanılan depremler gerçek kesitlerle gösterilmemiştir. Sayılar Çizelge 1'dekilerle aynıdır.

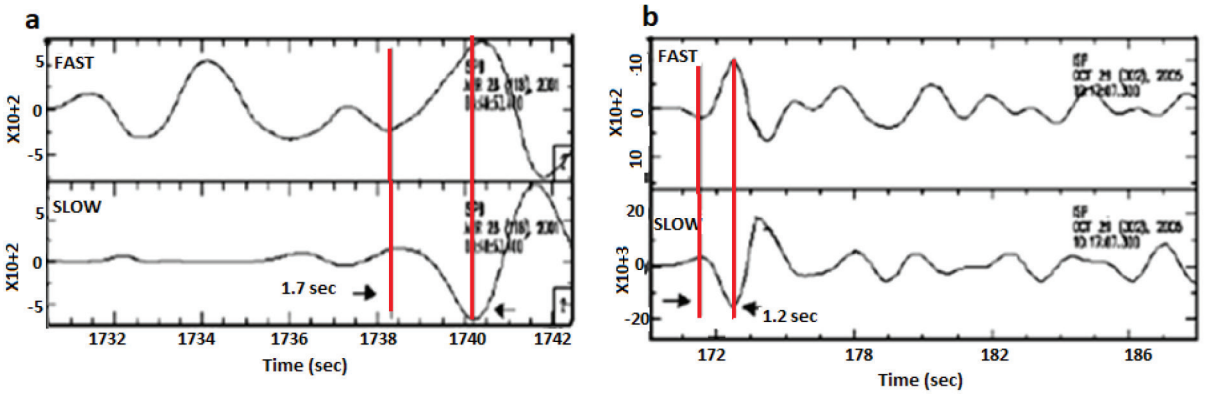

Figure 5. (a) An SKS wave recorded at station ISP and (b) a direct S wave (Event ID). The red lines show time window on traces for SKS and the direct S phases. The beginning and end time of the measurement window was manually picked. Amplitudes on all seismograms are traced-normalized within the selected time window.

Şekil 5. (a) İstasyon ISP'de kaydedilen bir SKS dalgası ile (b) doğrudan bir S dalgası (Olay ID 07). Kırmızı çizgiler SKS ve doğrudan gelen S fazlarının zaman penceresini göstermektedir. Ölçüm penceresinin başlangıcı ve bitiş zamanı el ile seçilmiştir. Tüm sismogramlardaki genlikler, seçilen zaman aralığında normalize edilerek çizilmiştir.

Table 1. Events used for local S wave.

Çizelge 1. Yerel S dalgası için kullanılan depremler.

ID	Year	Julday	Hr/mn	Lat. (deg)	Lon.(deg)	Depth (km)	Mb
01	2005	329	093056.90	35.02	23.32	32	5.2
02	2006	099	232719.81	35.17	27.24	32	5.10
03	2006	046	104118.50	36.16	23.37	64	4.50
04	2006	008	113455.64	36.31	23.21	66	6.70
05	2005	134	234650.53	35.69	31.58	69	5.10
06	2006	251	223910.40	36.37	27.71	77	4.50
07	2005	302	101707.30	35.46	22.44	80	4.60
08	2005	149	085535.80	38.26	22.73	104	5.00
09	2006	109	054042.30	36.67	26.94	131	4.70
10	2005	213	133500.20	36.57	26.78	133	5.00
11	2005	186	102925.10	36.53	27.07	139	4.60
12	2006	225	103512.70	34.42	26.57	32	5.20

study we overcome this problem by using this way that is based on measuring depth distribution of seismic anisotropy by studying the shear wave splitting of S waves generated from intermediate and shallow earthquakes (Figure 5 and Table 1). According to this approach, if azimuthal seismic anisotropy is evenly distributed with respect to depth, upgoing S waves originating from deeper hypocenters will have larger lag times than S waves originating from shallower earthquakes. It suggests that the lag times from the upgoing split S wave might be used to place some constraints on the depth of azimuthal anisotropy in the subducted slab and the overlying mantle wedge.

Results

The fast polarization directions of nearly all the stations at the southern margin of Peloponnese are oriented NW-SE and are parallel to the Hellenic Arc. Although the delay times of ISP and ANTB stations are different from HDMB, DALT, FETY and BODT stations shown in Figure 2, their fast polarization directions are all oriented NW-SE. In addition, we found that the fast polarization directions at stations ANTB and BALB are not parallel to the Cyprus Arc. Analyses of local S waves recorded by station BALB yield an average fast direction of NE-SW and lag time of approximately 1 sec (Table 2 and Figure 6). In addition to this, the measured local S wave splitting results at BALB are significantly consistent with finite strain related to the subducted slab (Figure 6 and Table 2) because finite strain developed within the subducted slab is related to time-dependent deformation (e.g., Li et al., 2014).

The fast polarization directions obtained from station ISP are not uniformly consistent, but they are compatible with the geometry of the slab (see Figure 2). However, the difference in lag times from local, teleseismic S and core refracted SKS/SKKS phases is 0.5 (see Figure 5). It indicates a significant amount of seismic anisotropy located in the epicentral depth.

Discussions and Conclusion

From the combined analyses of SKS, SKKS, local S, and teleseismic S waves, we conclude that seismic anisotropy is present in the mantle including the asthenosphere. Alternatively, an anisotropic layer would have to be present at the base of the 410 km discontinuity to produce the difference in the splitting parameters we observed. Although our data (Table 1) does not allow us to reach precise conclusions regarding the extent or distribution of anisotropy within the descending slab, comparison of local S wave splitting to SKS and SKKS splitting at our stations combined with the analysis of source-side anisotropy in the region seems to present compelling evidence of deep anisotropy below almost 100 km depth. Although the depth of anisotropy determined from the local S data is ambiguous, it is possible to combine local S splitting measurements with the teleseismic S and receiver-side splitting measurements to find the deep anisotropy residing within the slab.

Additionally, we suggest that the observed anisotropy at the subduction zone is unlikely due to metastable olivine because of its age (e.g., Ohtani et al., 2004). However, lattice preferred orientation of olivine minerals in the Western Anatolia is likely associated with the pervasive stretching of the Western Anatolian

Table 2. Shear wave splitting measurements from local S waves for BALB. ϕ and $\delta\tau$ show fast polarization direction and delay time, respectively. Baz is the back-azimuth (deg) and DF is the estimated error of the fast polarization direction.

Çizelge 2. Yerel S dalgasından BALB istasyonu için elde edilen kesme dalgası ayrımlanma ölçümleri. ϕ ve $\delta\tau$ sırasıyla hızlı polarizasyon yönü ve gecikme süresini gösterir. Baz: geri azimut açısı; DF: hızlı polarizasyon yönünün tahmini hatası.

ID	Julday	Φ(deg) ± DF	$\delta\tau$(s) ± error	Baz (deg)	Dist (deg)	Depth(km)
01	329	-39.47+/-14	1.10+/-0.05	219.64	5.87	32
02	099	83.04+/-19	1.25+/-0.10	186.71	4.49	32
03	046	-20.44+/-14	1.00+/-0.14	227.16	4.98	64
04	008	-10.99+/-7	1.20+/-0.05	229.44	4.97	66
05	134	61.63+/-15	1.40+/-0.45	142.19	4.92	69
07	302	-24.01+/-17	0.64+/-0.20	252.70	6.01	80
08	149	34.14+/-15	1.25+/-0.10	194.69	6.44	104
09	109	-64.93+/-21	1.16+/-0.14	194.32	3.06	131
10	213	10.42+/-124	1.16+/-0.10	196.15	3.19	133

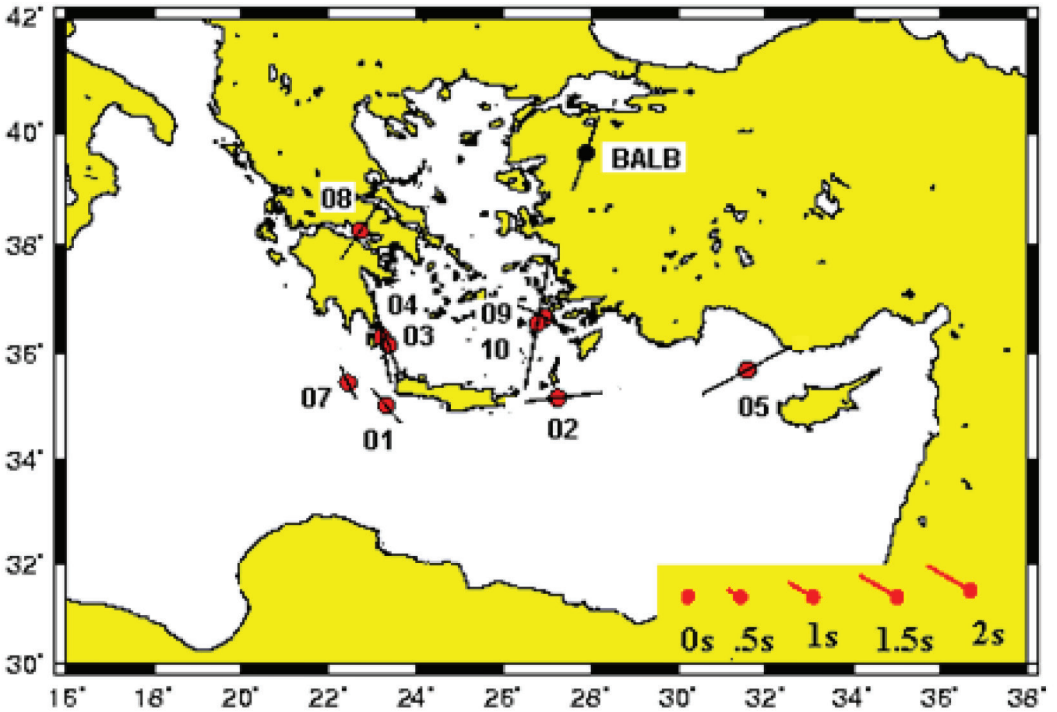

Figure 6. Local S waves splitting parameters (source side) beneath station BALB.
Şekil 6. İstasyon BALB' deki kaynak-yanı lokal S dalgası ayrımlanma parametreleri.

lithosphere. Some of high pressure and high temperature (high P–T) experiments carried out by researchers (e.g., Kubo et al., 2002; Kawakatsu and Yoshioka, 2011) indicated that metastable olivine might persist in a cold core of a slab due to the low rate of reaction associated with the olivine to wadsleyite phase transformation because the expected reaction can be accelerated or decelerated depending on the amount of water present in the slab mantle.

Although measured splitting parameters in the Cyprus arc (CA) (Figures 1 and 2) are not robust, it might be possible to suggest that seismic anisotropy within the CA is likely related to the present-day deformation. Hatzfeld et al. (2001) indicated that seismic anisotropy measured from SKS and SKKS teleseismic events measured at 25 stations deployed in the Aegean seems an inhomogeneous pattern. Meanwhile, an untidy pattern of Φ, similar to the splitting results of Hatzfeld et al. (2001), is observed at stations such as BALB. The consistency between the fast polarization directions of SKS (Hatzfeld et al., 2001) and local S waves suggests (see Figure 6) that the presence of anisotropy in the northwest part of the Hellenic subduction zone (Figure 1) is linked to coherent mantle flow. Besides, the measured small delay time in this region presumably is related to the deformation age of the subducted zone.

By this study, we concluded that azimuthal seismic anisotropy is present in the HSZ (the HSZ denoted as HA on Figure 1) and is related to slab break off (Faccenna et al., 2006). The orientations of local splitting fast directions in the Peloponnese Islands and surrounding areas are similar to those of Hatzfeld et al. (2001) and our SKS and SKKS results (Polat, 2006) (Figure 2). The consistency between the directions of the fast-polarized SKS waves and local S waves indicates that the presence of anisotropy in this region is linked to coherent mantle flow. However, we did not observe a similar consistency at the W-SW edge of the WA. This difference in splitting parameters for this part of the region may be related to complex asthenospheric flow beneath FETY, BODT, MLSB stations. Also, we observed that the fast polarization directions are uniform over the whole Aegean region.

Acknowledgements

We would like to thank Esen Arpat for his invaluable comments on geologic structure of the study area.

In particular, we thank Gülercan Selamioğlu for the English editing of this paper.

References

Ando, M., Ishikawa, Y. and Wada, H., 1980. S-wave anisotropy in the upper mantle under a volcanic area in Japan. Nature, 286, 43–46.

Ando, M., Ishikawa, Y., Yamazaki, F., 1983. Shear wave polarization anisotropy in the upper mantle beneath Honshu. Journal of Geophysical Research, 88, 5850–5864.

Backus, G. , 1962. Long-wave elastic anisotropy produced by horizontal layering. Journal of Geophysical Research, 67, 4427–4440.

Booth, D.C. and Crampin, S., 1985. Shear-wave polarizations on a curved wavefront at an isotropic free-surface. Geophysical Journal of the Royal Astronomical Society, 83, 31-45.

Christensen, N. I., 1984. The magnitude, symmetry and origin of up- per mantle anisotropy based on fabric analyses of ultramafic tectonics. Geophysical Journal of the Royal Astronomical Society, 76, 89-112.

Crampin, S., 1978. Seismic wave propagation through a cracked solid: polarization as a possible dilatancy diagnostic. Geophysical Journal of the Royal Astronomical Society, 53, 467-496.

Cochran, E. S., Vidale, J. E., and Li, Y. G., 2003. Near-fault anisotropy following the Hector Mine earthquake. Journal of Geophysical Research, 108, 2436, doi: 10.1029/2002JB002352.

Di Leo, J., Walker, A., Li, Z.-H., Wookey, J., Ribe, N., Kendall, J.-M. and Tommasi, A., 2014. Development of texture and seismic anisotropy during the onset of subduction. Geochemistry, Geophysics, Geosystems, 15, 192–212, doi:10.1002/2013GC005032.

Eakin, C.M., Long, M.D.,Wagner, L.S., Beck, S.L., Tavera, H., 2015. Upper mantle anisotropy beneath Peru from SKS splitting: Constraints on flat slab dynamics and interaction with the Nazca Ridge. Earth and Planetary Science Letters, 412:152–162. http://dx.doi.org/10.1016/j.epsl.2014.12.015.

Evangelidis, C., Liang, W., Melis, N. S. and Konstantinou, K. I., 2011. Shear wave anisotropy beneath the Aegean inferred from SKS splitting observations. Journal of Geophysical Research, 116, B04, 314, doi: 10.1029/2010JB007884.

Faccenna, C., Bellier, O., Martinod, J., Piromallo, C., and Regard, V., 2006. Slab detachment beneath eastern Anatolia: A possible cause for the formation of the North Anatolian fault. Earth and Planetary Science Letters, 242, 85–97.

Faccenda, M., and Capitanio, 2012. Development of mantle seismic anisotropy during subduction-induced 3-D flow. Geophysical Research Letters, 39, L11305, doi: 10.1029/2012GL051988.

Faccenda, M., and Capitanio, F., 2013. Seismic anisotropy around subduction zones: Insights from three-dimensional modeling of upper mantle deformation and SKS splitting calculations. Geochemistry, Geophysics, Geosystems, 14, 243–262, doi:10.1002/ggge.20055.

Hall, C. E., Fischer, K. M., Parmentier, E. M., and Blackman, D. K., 2000. The influence of plate motions on three-dimensional back arc mantle flow and shear wave splitting, Journal of Geophysical Research, 105(B12), 28009–28033, doi:10.1029/2000JB900297.

Hatzfeld, D., 2001. Shear wave anisotropy in the upper mantle beneath the Aegean related internal deformation, Journal of Geophysical Research: Solid Earth, 106, 30 737-30 754.

Karato, S.-I., Zhang, S. and Wenk, H.-R., 1995. Super-plasticity in the Earth's lower mantle:

Evidence from seismic anisotropy and rock physics, Science, 270, 458–461.

Karato, S. , 2008. Deformation of Earth Materials: Introduction to the Rheology of the Solid

Earth, 462. pp., Cambridge University Press, Cambridge, U.K.

Kawakatsu, H.,and Yoshioka, S., 2011. Metastale olivine wedge and deep dry cold slab beneath southwest Japan, Earth and Planetary Science Letters, 303, 1-10,doi:10.1016/j.epsi.2011.01.008.

Kubo, T., Ohtani, E., Kato, T., Urakawa, S., Suzuki, A., Kanbe, Y., Funakoshi, K., Utsumi, W., Kikegawa, T., Fujino, K., 2002. Mechanisms and kinetics of the post–spinel transformation in Mg2SiO4. Physics of the Earth and Planetary Interiors, 129, 153–171.

Li, Z.-Hai., Di Leo, J.F., and Ribe, N. M., 2014. Subduction-induced mantle flow, finite strain, and seismic anisotropy: Numerical modeling. Journal of Geophysical Research: Solid Earth, 119, 5052–5076, doi:10.1002/2014JB010996.

Long, M.D. and van der Hilst, R.D., 2005. Upper mantle anisotropy beneath Japan from shear wave splitting. Physics of the Earth and Planetary Interiors, 151, 206–222.

Long, M. and Silver, P. G., 2009. Shear wave splitting and mantle anisotropy: measurements, interpretations, and new directions. Surveys in Geophysics, 30, 407–461.

Lynner, C., and Long, M. D., 2014. Sub-slab anisotropy beneath the Sumatra and circum-Pacific subduction zones from source-side shear wave splitting observations. Geochemistry, Geophysics, Geosystems, 15, doi: 10.1002/2014GC005239.

Lynner, C., Long, M.D., Thissen, C.J., Paczkowski, K., and Montési, L.G.J., 2017. Evaluating geodynamic models for sub-slab anisotropy: Effects of olivine fabric type. Geosphere, v. 13, no. 2, p. 247–259, doi:10.1130/GES01395.1.

Mainprice, D., 2007. Seismic anisotropy of the deep Earth from a mineral and rock physics

perspective, in Treatise on Geophysics, vol. 2, edited by G. Schubert, pp. 437–492, Elsevier, Oxford, U.K.

Meissner, R., Rabbel, W., and Kern, H., 2006. Seismic lamination and anisotropy of the Lower Continental Crust. Tectonophysics, 416, 81–99.

Nuttli, O., 1961. The effects of the Earth's surface on the S wave particle motion. Bulletin of the Seismological Society of America, 51, 237–246, 1961.

Ohtani, E., Litasov, K., Hosoya, T., Kubo, T. and Kondo, T., 2004. Water transport into the deep mantle and formation of a hydrous transition zone. Physics of the Earth and Planetary Interiors, 143, pp.255-269.

Polat, G., 2006. Shear wave splitting for Turkey, M.S. in Geophysics Department, Bogazici University Kandilli Observatory and Earthquake Research Institute, Istanbul-Turkey.

Polat, G., Ozel, N. M., Crampin, S., Ergintav, S., and Tan, O.: Shear wave splitting as a proxy for stress forecast of the case of the 2006 Manyas-Kus Golu (Mb = 5.3) earthquake, Natural Hazards and Earth System Sciences, 12, 1073-1084, doi:10.5194/nhess-12-1073-2012.

Russo, R. M., and Silver, P. G., 1994. Trench-parallel flow beneath the Nazca plate from seismic anisotropy, Science, 263, 1105–1111.

Savage, M. K., 1999. Seismic anisotropy and mantle deformation: What have we learned from shear wave splitting?, Reviews of Geophysics, 37, 65–106, doi:10.1029/98RG02075.

Shih, O. R. and Meyer, P. R., 1990. Observation of Shear Wave Splitting From Natural Events "South Moat of Long Valley Caldera", California, June 29 to August 12, 1982, Journal of Geophysical Research, 95, 11179–11195.

Silver, P.G. and Chan, W. W., 1991. Shear wave splitting and subcontinental mantle deformation, Journal of Geophysical Research, 96, 16429-16454.

Silver, P. G., 1996. Seismic Anisotropy Beneath the Continents: Probing the Depths of Geology. Annual Review of Earth and Planetary Sciences, 24, 385–432, doi:10.1146/annurev.earth.24.1.385.

Vauchez, A., Tommasi A., Barruol, G., and J. Maumus, J., 2000. Upper mantle deformation and seismic anisotropy in continental rifts, Physics and Chemistry of the Earth V. 25, 111–117.

Teanby, N., Kendall, J.-M. , Jones, R. H. and Barkved, O., 2004. FAST TRACK PAPER: Stress induced temporal variations in seismic anisotropy observed in microseismic data. Geophysical Journal International, 156, 459–466, doi:10.1111/j.1365-246X.2004.02212.x.

Zatsepin, S. V. and Crampin, S., 1997. Modelling the compliance of crustal rock: I-response of shear-wave splitting to differential stress,

Geophysical Journal International, 129, 477–494.

Zhang, S., and Karato, S., 1995. Lattice preferred orientation of olivine aggregates deformed in simple shear. Nature, 375, 774–777.

Zimmerman, M.E., Zhang, S., Kohlstedt, D.L., Karato, S., 1999. Melt distribution in mantle rocks deformed in shear. Geophysical Research Letters 26, 1505–1508.